

A Samplable Multimodal Observation Model for Global Localization and Kidnapping

Runjian Chen¹ Yue Wang¹ Huan Yin¹ Yanmei Jiao¹
Gamini Dissanayake² Rong Xiong¹

¹CSE at Zhejiang University {rjchen, ywang24, zjuyinhuan, ymjiao, rxiong}@zju.edu.cn

²CAS at University of Technology, Sydney {Gamini.Dissanayake}@uts.edu.au

Abstract: Global localization and kidnapping are two challenging problems in robot localization. The popular method, Monte Carlo Localization (MCL) addresses the problem by sampling uniformly over the state space, which is unfortunately inefficient when the environment is large. To better deal with the problems, we present a proposal model, named Deep Multimodal Observation Model (DMOM). DMOM takes a map and a 2D laser scan as inputs and outputs a conditional multimodal probability distribution of the pose, making the samples more focusing on the regions with higher likelihood. With such samples, the convergence is expected to be much efficient. Considering that learning based Samplable Observation Model may fail to capture the true pose sometimes, we furthermore propose the ADAPTIVE MIXTURE MCL, which adaptively selects updating mode for each particle to tolerate this situation. Equipped with DMOM, ADAPTIVE MIXTURE MCL can achieve more accurate estimation, faster convergence and better scalability compared with previous methods in both synthetic and real scenes. Even in real environment with long-term changing, ADAPTIVE MIXTURE MCL is able to localize the robot using DMOM trained only on simulated observations from a SLAM map, or even a blueprint map.

Keywords: Global Localization, Samplable Observation Model, Multimodal

1 Introduction

The ability to accurately localize a robot is the fundamental requirement for many robotics applications, including motion planning, decision making and control [1, 2, 3, 4]. In this paper, we focus on the global localization and kidnapping problem on 2D scenes with 2D laser observation. Given real-time motion information and 2D laser observation, the goal of global localization is to estimate the pose of the robot with respect to a map of the environment without any prior about the robot pose. In the kidnapping problem, where the robot is suddenly taken to some other place without being told, the algorithm should be able to detect this situation and recover from it.

Out of the conventional frameworks for robot localization, including [5, 6, 7, 8], Monte Carlo Localization (MCL) is arguably the most popular and efficient one [9] for the global localization and kidnapping problem. MCL uses a set of particles to represent the estimated probability distribution of the robot pose and iteratively deploys Bayes rule to update this set with the Motion Model and Observation Model. In [7, 10, 11], variants of MCL are proposed to boost its performance, among which MIXTURE MCL [7] achieves the best performance. The key to the success of MIXTURE MCL is DUAL MCL with a handcrafted-feature-based Samplable Observation Model, which can use handcrafted features of observation to provide a probability distribution over state space for sampling particle while traditional MCL is only able to sample from a uniform distribution. However, when working in an environment that is highly symmetrical or dynamic, MIXTURE MCL still faces the problem of high computation cost and unsatisfactory estimation accuracy of localization. The bottleneck lies in the inaccurate Samplable Observation Model. First of all,

the three handcrafted features in [7] are not able to extract enough meaningful information from the laser ranges, resulting in an imprecise probability distribution. Also, MIXTURE MCL requires physical data collection in the testing environment, which is sometimes not applicable in the real application and limits its generalization ability.

As deep learning techniques can learn a model in a data-driven mode and generalize across datasets, there comes a surge of deep learning models that can be used to construct `Samplable Observation Models`. They can be classified into the following two categories by how many probability peaks they provide.

- (1) **Unimodal:** Represented by [12, 13], a classifier or a regression network is trained to find the pose with the largest possibility to obtain the observation in a given map, which provides only a unimodal distribution. Intuitively, due to the fact that the robot can appear on only one pose at a timestamp, a perfect `Samplable Observation Model` should be unimodal. However, as the environment can be very symmetrical and dynamic (with people walking around or unknown obstacles), observation can be very similar and correspond to several robot poses. Under this kind of situation, unimodal distribution might easily lose track of the robot pose.
- (2) **Top N:** Embraced by [14, 15, 16], this kind of methods train deep models to extract features of the RGB or 3D point cloud information and features of templates in the database, with which they are able to propose top N possible poses of the robot. There are two limitations in this category. First, it can only choose the top N regions, where N is a fixed handcrafted parameter. However, in real scenes, an observation might correspond to different numbers of poses and N limits the flexibility of this model to approximate the true multimodal distribution. Secondly, the output of this kind of model is simply N regions and additional effort should be taken to construct a probability distribution over the state space.

Thus a good `Samplable Observation Models` should be able to provide an accurate multimodal probability distribution with adaptive number of probability peaks. Besides, generalization ability, low time consumption and scalability over scene sizes are also important requirements. Moreover, as training samples for `Samplable Observation Models` may not cover every possible situation, the predicted probability distribution can sometimes fail to capture the correct pose. As MIXTURE MCL deploys traditional MCL with a probability of p_{MCL} or DUAL MCL with a probability of $1 - p_{MCL}$ in every updating iteration, the particle set must lose track of the robot pose if MIXTURE MCL barely use the DUAL MCL branch under the case above.

To address these challenges, we propose the Deep Multimodal Observation Model (DMOM) and ADAPTIVE MIXTURE MCL. As shown in Figure 1, DMOM first aggregates features of the observation and a pre-built map without obstacles, and then computes their similarity, followed by a distribution decoder to lift the similarity matrix to a probability distribution over the state space with adaptive number of probability peaks. Different from the way in which MIXTURE MCL combines the traditional MCL and DUAL MCL, ADAPTIVE MIXTURE MCL first divides the whole particle set into highly trusted set and untrusted set and then deploys traditional MCL and DUAL MCL with DMOM respectively for these two parts. Experiments demonstrate that DMOM has the ability to generalize across different synthetic environments. In real environments, DMOM can be trained by only simulation laser scans in given SLAM-based or floorplan maps and applied to infer the probability distribution with real 2D laser scans. Detailed experiments in both synthetic and real environments demonstrate that ADAPTIVE MIXTURE MCL outperforms MCL and MIXTURE MCL in both effectiveness and efficiency, even when the `Samplable Observation Models` in MIXTURE MCL is trained by data containing the testing sequences. Even in real, highly dynamic environments like a palace, ADAPTIVE MIXTURE MCL is able to accurately localize the robot.

2 Problem Formulation

We use $s_t = (x_t, y_t, \theta_t)$ to denote the state (pose) of the robot at timestamp t , where (x_t, y_t) is the position and θ_t indicates the orientation. $Bel(s_t)$ is the probability distribution of s_t . We use

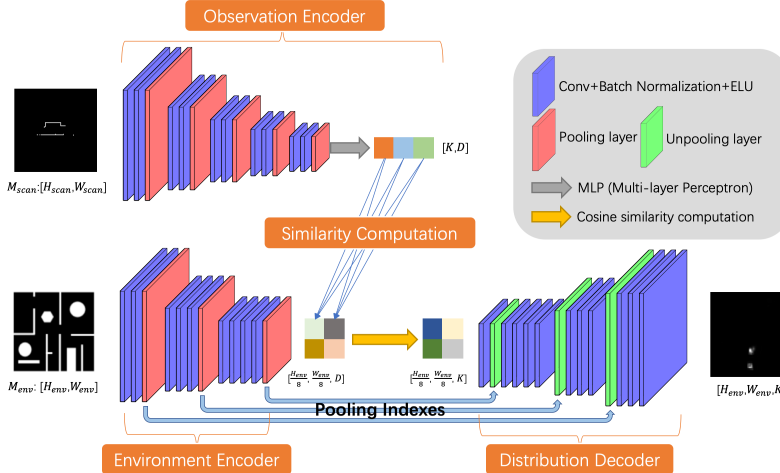


Figure 1: The architecture of Deep Multimodal Observation Model.

\mathbf{M}_{env} to denote the occupancy matrix for the environment and a_t and o_t respectively for the motion and observation information (2D laser scan in our setting) at timestamp t . Note that a_{t-1} is the control command executed during the time interval $[t-1, t]$. Then as shown in (1), the problem is to estimate $Bel(s_t)$ with given sequences of observation and motion information.

$$Bel(s_t) = p(s_t | o_{0:t}, a_{0:t-1}, \mathbf{M}_{env}) \quad (1)$$

Based on Recursive Bayes Filtering, Monte Carlo Localization [7] transforms (1) into (2) with an Markov assumption and Bayes Theorem [17] [18]. In (2), η is the normalization term, $p(o_t | s_t, \mathbf{M}_{env})$ stands for the Observation Model, $p(s_t | s_{t-1}, a_{t-1}, \mathbf{M}_{env})$ describes the Motion Model and $Bel(s_{t-1})$ indicates the Prior (distribution at the last timestamp).

$$Bel(s_t) = \eta p(o_t | s_t, \mathbf{M}_{env}) \int p(s_t | s_{t-1}, a_{t-1}, \mathbf{M}_{env}) Bel(s_{t-1}) ds_{t-1} \quad (2)$$

To approximate $Bel(s_t)$, MCL [7] uses a set of particles $\mathcal{P}_t = (s_t^i, w_t^i)$, where s_t^i is the state of the i^{th} particle and w_t^i is the weight of it at timestamp t . Beginning with random sampling over the state space, MCL iteratively updates the particle set from the previous timestamp by the following steps:

- (1) **Sampling:** Sample \mathcal{P}_t from \mathcal{P}_{t-1} according to w_{t-1}^i and update particle states in \mathcal{P}_t with a_{t-1} .
- (2) **Weighting:** Reweight particles in \mathcal{P}_t with Weighting Observation Model.

DUAL MCL is a “reverse” version of MCL, which deploys three handcrafted features to train a kd-tree as a Samplable Observation Model. To start with, observation data in the same scene are collected and the features of these data are computed to form the Samplable Observation Model. Then DUAL MCL follows the steps below to update the particle set:

- (1) **Sampling:** Compute features of o_t and sample \mathcal{P}_t with the Samplable Observation Model.
- (2) **Weighting:** Find related particles in \mathcal{P}_{t-1} for each particle in \mathcal{P}_t with a_{t-1} and set the weights of particles \mathcal{P}_t the same as those of related particles.

The most important difference between DUAL MCL and traditional MCL lies in the way they sample the new particle set. Traditional MCL starts from uniform distribution across the state space while DUAL MCL is able to sample from a multimodal prior. However, the Samplable Observation Model might be unstable. Thus MIXTURE MCL combines both to achieve a relatively satisfying performance on global localization and kidnapping problems.

3 Deep Multimodal Observation Model

In this section, we propose our Deep Multimodal Observation Model (DMOM). As shown in Figure 1, the inputs of DMOM are two images, one for the environment and one for the observation information (here we transform the 2D laser ranges to a 2D image), represented by two matrices $\mathbf{M}_{env} \in \mathbb{R}^{H_{env} \times W_{env}}$ and $\mathbf{M}_{scan} \in \mathbb{R}^{H_{scan} \times W_{scan}}$. \mathbf{PM} , the output of DMOM, is the grid approximation of the probability distribution of the robot pose. We discretize the state space (x, y, θ) by $[H_{env}, W_{env}, K]$ and each entry in the matrix $\mathbf{PM} \in \mathbb{R}^{H_{env} \times W_{env} \times K}$ stands for the probability that the robot gets the observation \mathbf{M}_{scan} on the exact pose. DMOM consists of four main parts: (1) observation encoder (2) environment encoder (3) similarity computation (4) distribution decoder. Section 3.1 shows details in these four parts and the loss function. Then we explain why DMOM can approximate the multimodal probability distribution in Section 3.2.

3.1 Architecture

Observation Encoder. As described in (3), F_{enc}^{scan} is first deployed to encode \mathbf{M}_{scan} to a feature map and then a Multi-Layer Perceptron (*MLP*) transforms this feature map to the feature representation $\mathbf{S} \in \mathbb{R}^{K \times D}$. We can see that there are K feature vectors in \mathbf{S} , each of which is related to the feature at each discretized rotation angle. As illustrated in Figure 1, F_{enc}^{scan} consists of several encoding blocks, which contains convolutional layers, batch normalization layers, non-linear activation layers and pooling layers.

$$\mathbf{S} = MLP(F_{enc}^{scan}(\mathbf{M}_{scan})) \quad (3)$$

Environment Encoder. As (4) shows, F_{enc}^{env} , which is similar to F_{enc}^{scan} , transforms the map of the environment $\mathbf{M}_{env} \in \mathbb{R}^{H_{env} \times W_{env}}$ to its feature map $\mathbf{M} \in \mathbb{R}^{\frac{H_{env}}{8} \times \frac{W_{env}}{8} \times D}$.

$$\mathbf{M} = F_{enc}^{env}(\mathbf{M}_{env}) \quad (4)$$

Similarity Computation. Cosine similarity is deployed to compute the similarity between \mathbf{S} and \mathbf{M} , resulting in the similarity feature map $\mathbf{SIM} \in \mathbb{R}^{\frac{H_{env}}{8} \times \frac{W_{env}}{8} \times K}$. As described in (5), $\mathbf{S}_k \in \mathbb{R}^D$ is the k^{th} feature vector in \mathbf{S} , $\mathbf{M}_{i,j} \in \mathbb{R}^D$ is the feature vector on pixel (i, j) on \mathbf{M} and ϵ is a very small number to avoid dividing by zero. $\mathbf{SIM}_{i,j,k}$ indicates the (i, j, k) entry in \mathbf{SIM} .

$$\mathbf{SIM}_{i,j,k} = \frac{\mathbf{S}_k^T \mathbf{M}_{i,j}}{\max(\|\mathbf{S}_k\|_2 \cdot \|\mathbf{M}_{i,j}\|_2, \epsilon)} \quad (5)$$

Distribution Decoder. In (6), F_{dec} and a softmax activation σ lift \mathbf{SIM} to \mathbf{PM} , which stands for the grid approximation of probability distribution over the state space. F_{dec} consists of several decoding blocks, each of which contains convolutional layers, batch normalization layers, non-linear activation layers and an unpooling layer. The unpooling indexes are the same as the pooling indexes in the environment encoder.

$$\mathbf{PM} = \sigma(F_{dec}(\mathbf{SIM})) \quad (6)$$

Loss Function. To help the network better capture the useful information for probability distribution generation, Kullback-Leibler divergence Loss [19] (KLD Loss) is deployed to guide the training process of the network. A unimodal probability distribution at the exact pose where the robot obtains the observation is computed as the ground truth, \mathbf{GT} . Details about the generation of \mathbf{GT} are shown in Appendix C. (7) illustrates how KLD Loss works, where $\mathbf{GT}_{i,j,k}$ and $\mathbf{PM}_{i,j,k}$ respectively indicate the (i, j, k) entry in \mathbf{GT} and \mathbf{PM} .

$$Loss = \sum_{i=1}^{H_{env}} \sum_{j=1}^{W_{env}} \sum_{k=1}^K \left[\mathbf{GT}_{i,j,k} \log \frac{\mathbf{GT}_{i,j,k}}{\mathbf{PM}_{i,j,k}} \right] \quad (7)$$

3.2 Multi-Modal Effect in DMOM

Why can the unimodal ground truth guide the network to generate a multimodal probability distribution? Assuming that there exists a set of similar observations $\{\mathbf{M}_{scan}^l | l = 1, 2, \dots, m\}$ obtained

at a set of different states (poses) $\{s^l | l = 1, 2, \dots, m\}$ in the training set, all the \mathbf{S} generated by observation encoder are extremely similar while environment encoder should obtain the same feature map \mathbf{M} , resulting in a set of highly similar probability map $\{\mathbf{PM}^l | l = 1, 2, \dots, m\}$. The sum of the KLD Losses of these m samples is minimized only when the output \mathbf{PM} is an even-distributed multimodal distribution on these m poses.

We here prove the case in which $\{\mathbf{GT}^l | l = 1, 2, \dots, m\}$ are one-hot (1 at the ground truth pose and 0s at other entries) and \mathbf{M}_{scan}^l are the same. Thus all the \mathbf{PM}^l are the same, denoted as \mathbf{PM} . The sum of losses is described in (8), where \mathbf{PM}_{s^l} indicates value on the entry s^l of \mathbf{PM} .

$$\begin{aligned} Loss &= \sum_{l=1}^m \left\{ \sum_{i=1}^{H_{env}} \sum_{j=1}^{W_{env}} \sum_{k=1}^K \left[\mathbf{GT}_{i,j,k}^l \log \frac{\mathbf{GT}_{i,j,k}}{\mathbf{PM}_{i,j,k}} \right] \right\} \\ &= \sum_{l=1}^m -\log \mathbf{PM}_{s^l} \end{aligned} \quad (8)$$

Thus the problem turns to:

$$\begin{aligned} &\underset{\mathbf{PM}}{\text{minimize}} \quad \sum_{l=1}^m -\log \mathbf{PM}[s^l] \\ &\text{subject to} \quad \sum_s \mathbf{PM}_s = 1 \end{aligned} \quad (9)$$

After applying Lagrange multiplier to it, the problem turns to minimize the term below:

$$\underset{\mathbf{PM}, \lambda}{\text{minimize}} \quad L = \sum_{l=1}^m -\log \mathbf{PM}_{s^l} + \lambda \left(1 - \sum_s \mathbf{PM}_s \right) \quad (10)$$

Let the derivative of L with respect to every entry in \mathbf{PM} and λ be 0, we get:

$$\begin{aligned} \frac{1}{\lambda} &= \mathbf{PM}_{s^1} = \mathbf{PM}_{s^2} = \dots = \mathbf{PM}_{s^m} \\ \mathbf{PM}_s &= 0, \quad \forall s \notin \{s^l | l = 1, 2, \dots, m\} \end{aligned} \quad (11)$$

Also with $\sum_s \mathbf{PM}_s = 1$, we can get that only when $\mathbf{PM}_{s^1} = \mathbf{PM}_{s^2} = \dots = \mathbf{PM}_{s^m} = \frac{1}{m}$ can the sum of these m KLD Losses get minimized. As training samples can cover part of the state space, it is obvious that the KLD Loss is able to guide the network to approximate the ground truth multimodal distribution.

4 Adaptive Mixture MCL

As training data is not able to cover the whole state space, \mathbf{PM} sometimes fails to approximate the accurate probability distribution. To compensate this problem, we propose a novel filter, ADAPTIVE MIXTURE MCL, which deploys \mathbf{PM} as a `Samplable Observation Model`, to tackle with the global localization as well as kidnapping problem.

In ADAPTIVE MIXTURE MCL, each particle has three elements (s^i, w_{norm}^i, w^i) , where the first one indicates the pose of this particle, w^i is the original observation weight from the `Weighting Observation Model` and w_{norm}^i is the normalized weight. In every updating iteration, we first evaluate the degree we trust a particle by computing $\frac{w^i}{w_{perfect}}$, where $w_{perfect}$ is the weight of ‘‘perfect observation’’ (the same as we can obtain in the given map of the environment). According to the values computed in the previous step, we divide the whole set into \mathcal{H} and \mathcal{L} . To endure noise in the observation, we introduce a parameter $w_{cut} \in (0, 1)$ and if $\frac{w^i}{w_{perfect}} > w_{cut}$, we directly add this particle to \mathcal{H} . If not, this particle is added to \mathcal{H} with a probability of $\frac{w^i}{w_{perfect}}$ or \mathcal{L} with a probability of $1 - \frac{w^i}{w_{perfect}}$. Finally we deploy normal MCL update for \mathcal{H} and DUAL MCL update with \mathbf{PM} for \mathcal{L} . An algorithm of ADAPTIVE MIXTURE MCL is shown in Appendix A.

5 Experiments and Results

In this section, we conduct extensive experiments in both synthetic and real scenes to investigate the following three questions: 1) How well does DMOM approximate the multimodal probability distribution? 2) How well does ADAPTIVE MIXTURE MCL solve the global localization and kidnapping problem? 3) What kind of generalization ability does ADAPTIVE MIXTURE MCL have?

5.1 Experiments Setup

Environments. For synthetic environments, we manually create 20 maps. We collect training data in 18 of them and testing sequences in the other 2 maps. To train DMOM, we add random obstacles in the environments and simulate laser to get the observation. What we feed into DMOM are the original map without obstacles and the observation. For the testing sequential data, we put unknown obstacles or remove some parts of the environment along the path where the robot moves.

For real environments, we conduct experiments on two benchmark real-world dataset: the Royal Alczar of Seville dataset (UPO) [20] and the Rawseeds indoor dataset collected in the Universit di Milano-Bicocca (Bicocca) [21] [22]. For the Bicocca dataset, we divide the whole scene into two smaller parts for experiments. To train DMOM, we add random obstacles to the map given by these datasets (SLAM-based or floorplan) and collect training data using simulating laser. With these synthetic data, we train DMOM, after which it is applied to real observation in the same scene.

Settings in Baselines and Adaptive Mixture MCL. There are two types of baselines in our experiments: traditional MCL with random sampling and MIXTURE MCL [7]. As the `Weighting Observation Model` in these two baselines influences their performance a lot, we try several models introduced in [23] [24]. Also we try our best to tune the parameters in these two baseline for better performance than the original parameter set in [23] [24], leading to the final baselines. Note here that the `Samplable Observation Models` in MIXTURE MCL introduced in [7] is not robust and we use data containing testing sequences (except for the exact pose at a given timestamp) to train it, which to some extent is “cheating” because an algorithm should not have any prior about the testing sequences. We set the particle number to 500 for these two methods and ADAPTIVE MIXTURE MCL. The random sampling rate of traditional MCL is set to 0.2. The network structure in DMOM remains the same in different experiments to demonstrate the scalability of it. w_{cut} is set to 0.6. And results for parameter sensitivity experiments on w_{cut} are shown in Appendix B.

Evaluation Metric. For each testing sequence and method, we run experiments for 100 times. Then the error of the estimated position $(x_{est}, y_{est}, \theta_{est})$ is computed at each updating iteration as follow: $E_{pos} = \sqrt{(x_{est} - x_{gt})^2 + (y_{est} - y_{gt})^2}$ and $E_{rot} = \sqrt{(\theta_{est} - \theta_{gt})^2}$. Thus at each updating iteration on each testing sequence, we have 100 error values for each method.

To show the converging process of each method, we compute the mean value as well as 95% confidence interval of the 100 error values E_{pos} at each updating step and plot the changing estimation error of all methods on the same chart to compare their performance. To evaluate how accurate the algorithms converge, we do two “box plots” respectively for E_{pos} in global localization and kidnapping problems. To evaluate how fast and stable an algorithm converges, we first set a condition for converging to the accurate pose: If E_{pos} is lower than 1 meter and the error in orientation E_{rot} is lower than 10 degrees for 10 consecutive updating steps, we consider that the algorithm converges to the accurate pose. If an algorithm converges, $STEPS$ is computed as the number of steps from the beginning of the problem to the first step in these 10. Finally we deploy histogram to show the comparison on converging speeds and rates.

5.2 Visualization Results on the Output of DMOM

In Figure 2, it is clear that DMOM is able to take the observation and map without obstacles as inputs and generate different numbers of probability peaks including the ground truth, which demonstrates DMOM as an acceptable `Samplable Observation Model`

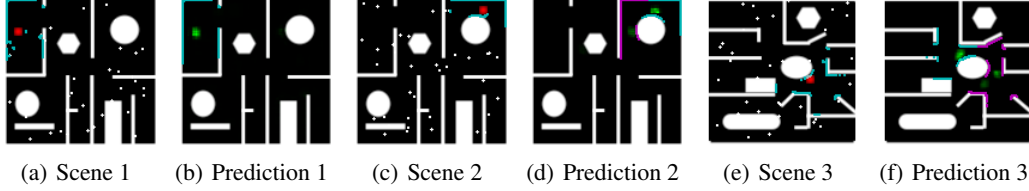


Figure 2: Visualization results on the output of DMOM. As shown in (a)(c)(e), observation with obstacles around is indicated by blue lines. Red squares in (a)(c)(e) indicate the ground truth position. The input of DMOM are observation in (a)(c)(e) and a “clean” map. Green clusters in (b)(d)(f) show the predicted probability peaks. Blue and purple lines in (b)(d)(f) show the observation on the predicted probability peaks. The size of the scene is 43 meters in both width and height.

5.3 Ablation Study

We compare four methods in a testing synthetic environment: MCL, MIXTURE MCL, Mixture MCL with DMOM as `Samplable Observation Model` and `ADAPTIVE MIXTURE MCL`. The results for global localization and kidnapping with these four methods are shown in Figure 3. It can be found that MIXTURE MCL and Mixture MCL with DMOM achieve similar performance while the `Samplable Observation Model` in the former one is “cheating”. This demonstrates that DMOM is able to generalize across synthetic environments and provide an accurate probability distribution over the state space for sampling. Also, it is obviously observed that Adaptive Mixture MCL converges faster and achieves more accurate estimation than Mixture MCL with DMOM, demonstrating the effectiveness of Adaptive Mixture MCL.

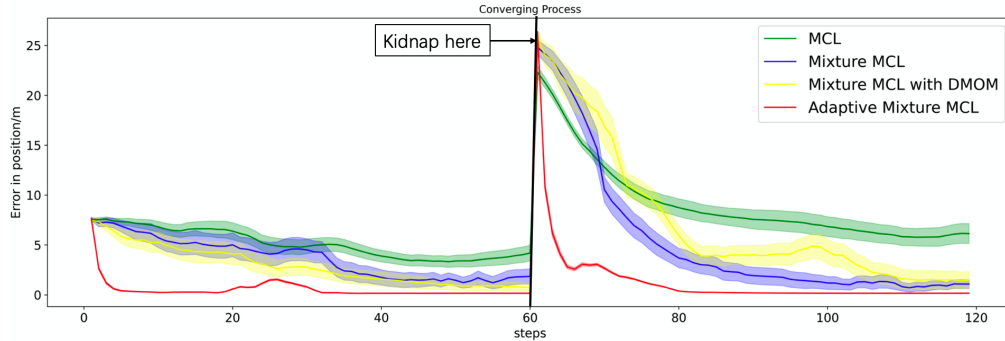


Figure 3: Results on the ablation study experiment.

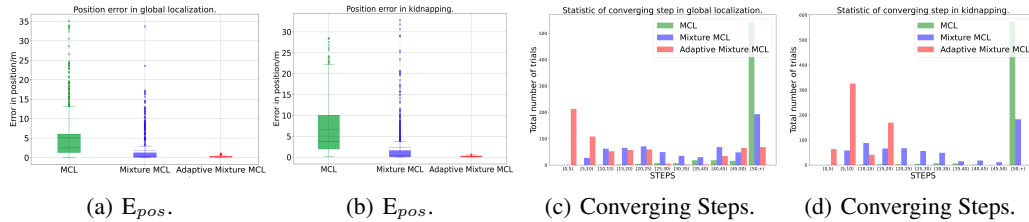
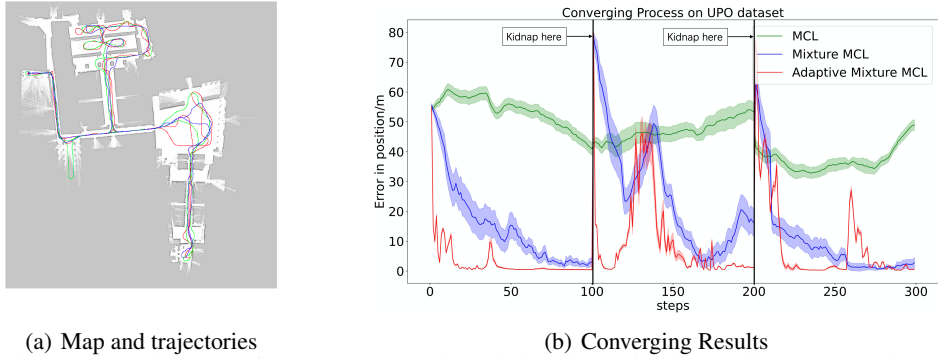


Figure 4: Results on synthetic environments. (a)(b) respectively show the results of E_{pos} in global localization and kidnapping problem. (c)(d) are histograms for converging steps among 600 experiments in global localization and kidnapping problem.

5.4 Results on Localization and Generalization

Train in some synthetic maps and test in “unseen” synthetic maps. Six sequences of synthetic data are collected in two synthetic maps to evaluate the performance of the three methods, leading to 600 experiments for each method. For each sequence of testing data, we first start from global localization and then kidnap the robot for one time. As shown in Figure 4, it can be found that `ADAPTIVE MIXTURE MCL` achieves significantly better estimation results than the other two. Also

ADAPTIVE MIXTURE MCL achieves the highest converging rate and requires least steps to converge. These demonstrate that DMOM is able to generalize across different synthetic environments and aid ADAPTIVE MIXTURE MCL to accurately localize the robot in “unseen” synthetic scenes.



(a) Map and trajectories (b) Converting Results
 Figure 5: (a) shows the map of UPO dataset and multiple trajectories they collect. We random select three testing clips among them. (b) shows the localization results.

Train with simulation observation on SLAM-based or floorplan maps and test on real observation. As shown in Figure 5 and 6, it can be found that under most cases in real scenes, ADAPTIVE MIXTURE MCL can achieve a more accurate estimation even than the MIXTURE MCL with a “cheating” Samplable Observation Model. These results indicate that DMOM can learn from synthetic laser range data in the given map of a real environment (SLAM-based or floorplan) and generalize to real observation in the same environment, which helps ADAPTIVE MIXTURE MCL to attain accurate estimation of the robot pose in real environments. We also notice that the results of the first experiment on the Bicocca dataset are not satisfying enough. We think the problem lies in that the real scene in this experiment may be very different from that of the floorplan.

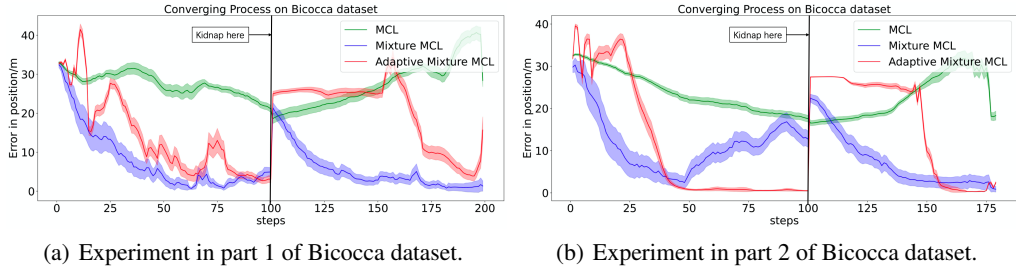


Figure 6: Results on Bicocca dataset

6 Conclusion

In this paper, we propose a samplable deep multimodal observation model, DMOM, as well as ADAPTIVE MIXTURE MCL, which is a novel localization filter for global localization and kidnapping problems. Our extensive experiments demonstrate that DMOM is able to generalize across different synthetic environments. Moreover it can generalize to real environments when trained on only simulated observations from a SLAM-based, or even blueprint maps.

Acknowledgments

If a paper is accepted, the final camera-ready version will (and probably should) include acknowledgments. All acknowledgments go at the end of the paper, including thanks to reviewers who gave useful comments, to colleagues who contributed to the ideas, and to funding agencies and corporate sponsors that provided financial support.

References

- [1] I. J. Cox. Blanche—an experiment in guidance and navigation of an autonomous robot vehicle. *IEEE Transactions on robotics and automation*, 7(2):193–204, 1991.
- [2] T. Fukuda, S. Ito, N. Oota, F. Arai, Y. Abe, K. Tanaka, and Y. Tanaka. Navigation system based on ceiling landmark recognition for autonomous mobile robot. In *Proceedings of IECON'93-19th Annual Conference of IEEE Industrial Electronics*, pages 1466–1471. IEEE, 1993.
- [3] R. Hinkel and T. Knieriemien. Environment perception with a laser radar in a fast moving robot. In *Robot Control 1988 (Syroco'88)*, pages 271–277. Elsevier, 1989.
- [4] J. J. Leonard, H. F. Durrant-Whyte, and I. J. Cox. Dynamic map building for an autonomous mobile robot. *The International Journal of Robotics Research*, 11(4):286–298, 1992.
- [5] G. Welch, G. Bishop, et al. An introduction to the kalman filter, 1995.
- [6] S. J. Julier and J. K. Uhlmann. New extension of the kalman filter to nonlinear systems. In *Signal processing, sensor fusion, and target recognition VI*, volume 3068, pages 182–193. International Society for Optics and Photonics, 1997.
- [7] S. Thrun, D. Fox, W. Burgard, and F. Dellaert. Robust monte carlo localization for mobile robots. *Artificial intelligence*, 128(1-2):99–141, 2001.
- [8] D. Fox, W. Burgard, F. Dellaert, and S. Thrun. Monte carlo localization: Efficient position estimation for mobile robots. In *Proceedings of the Sixteenth National Conference on Artificial Intelligence (AAAI'99)*, July 1999.
- [9] C. Stachniss and W. Burgard. Particle Filters for Robot Navigation. *Foundations and trends in Robotics*, 3(4):211–282, 2014. doi:10.1561/23000000013. URL <http://www.qjps.com/article/Download/ROB-013>.
- [10] K. Nummiaro, E. Koller-Meier, and L. Van Gool. An adaptive color-based particle filter. *Image and vision computing*, 21(1):99–110, 2003.
- [11] K. Okuma, A. Taleghani, N. De Freitas, J. J. Little, and D. G. Lowe. A boosted particle filter: Multitarget detection and tracking. In *European conference on computer vision*, pages 28–39. Springer, 2004.
- [12] G. Kim, B. Park, and A. Kim. 1-day learning, 1-year localization: Long-term lidar localization using scan context image. *IEEE Robotics and Automation Letters*, 4(2):1948–1955, 2019.
- [13] A. Kendall, M. Grimes, and R. Cipolla. Posenet: A convolutional network for real-time 6-dof camera relocalization. In *Proceedings of the IEEE international conference on computer vision*, pages 2938–2946, 2015.
- [14] S. Xu, W. Chou, and H. Dong. A robust indoor localization system integrating visual localization aided by cnn-based image retrieval with monte carlo localization. *Sensors*, 19(2):249, 2019.
- [15] M. Angelina Uy and G. Hee Lee. Pointnetvlad: Deep point cloud based retrieval for large-scale place recognition. In *Proceedings of the IEEE Conference on Computer Vision and Pattern Recognition*, pages 4470–4479, 2018.

- [16] H. Yin, Y. Wang, X. Ding, L. Tang, S. Huang, and R. Xiong. 3d lidar-based global localization using siamese neural network. *IEEE Transactions on Intelligent Transportation Systems*, 21(4):1380–1392, 2019.
- [17] J. M. Bernardo and A. F. Smith. *Bayesian theory*, volume 405. John Wiley & Sons, 2009.
- [18] A. R. Cassandra, L. P. Kaelbling, and J. A. Kurien. Acting under uncertainty: Discrete bayesian models for mobile-robot navigation. In *Proceedings of IEEE/RSJ International Conference on Intelligent Robots and Systems. IROS'96*, volume 2, pages 963–972. IEEE, 1996.
- [19] T. Van Erven and P. Harremos. Rényi divergence and kullback-leibler divergence. *IEEE Transactions on Information Theory*, 60(7):3797–3820, 2014.
- [20] R. Ramón-Vigo, J. Pérez, F. Caballero, and L. Merino. Navigating among people in crowded environment: Datasets for localization and human robot interaction. In *Proceedings of the Workshop on Robots in Clutter: Perception and Interaction in Clutter, IEEE/RSJ International Conference on Intelligent Robots and Systems (IROS)*. Citeseer, 2014.
- [21] S. Ceriani, G. Fontana, A. Giusti, D. Marzorati, M. Matteucci, D. Migliore, D. Rizzi, D. G. Sorrenti, and P. Taddei. Rawseeds ground truth collection systems for indoor self-localization and mapping. *Autonomous Robots*, 27(4):353, 2009.
- [22] A. Bonarini, W. Burgard, G. Fontana, M. Matteucci, D. G. Sorrenti, and J. D. Tardos. Rawseeds: Robotics advancement through web-publishing of sensorial and elaborated extensive data sets. In *In proceedings of IROS*, volume 6, page 93, 2006.
- [23] S. Thrun. Probabilistic robotics. *Communications of the ACM*, 45(3):52–57, 2002.
- [24] M. Quigley, K. Conley, B. Gerkey, J. Faust, T. Foote, J. Leibs, R. Wheeler, and A. Y. Ng. Ros: an open-source robot operating system. In *ICRA workshop on open source software*, volume 3, page 5. Kobe, Japan, 2009.

Appendices

A ADAPTIVE MIXTURE MCL

Algorithm 1 shows how ADAPTIVE MIXTURE MCL works. First, the particles in \mathcal{P}_{t-1} are divided into two sets: \mathcal{H} and \mathcal{L} by how well we trust them (line 6 to 16). w^i indicates the original weight (from Weighting Observation Model) of the i^{th} particle and w_{perfect} is the weight (from Weighting Observation Model) of a “perfect scan” (that is in each direction, the range from laser is the same as what we can observe in the given map). Then as illustrated in line 18 to 29, we deploy traditional MCL on \mathcal{H} and DUAL MCL on \mathcal{L} with PM, which is the output of DMOM.

Algorithm 1: Adaptive Mixture MCL

Input: $\mathcal{P}_{t-1}, o_t, a_{t-1}, w_{\text{perfect}}, \mathbf{M}_{\text{env}}, w_{\text{cut}}$

Output: \mathcal{P}_t

```

1 begin
2    $\text{PM} \leftarrow \text{DMOM}(o_t, \mathbf{M}_{\text{env}})$ 
3    $\mathcal{P}_t \leftarrow \emptyset$ 
4   /* Divide  $\mathcal{P}_{t-1}$  into  $\mathcal{H}$  and  $\mathcal{L}$ , respectively for highly trusted set of
5     particles and untrusted set of particles. */
6    $\mathcal{H} \leftarrow \emptyset$ 
7    $\mathcal{L} \leftarrow \emptyset$ 
8   for  $(s^i, w_{\text{norm}}^i, w^i) \in \mathbf{P}_{t-1}$  do
9     if  $\frac{w^i}{w_{\text{perfect}}} > w_{\text{cut}}$  then
10       $\mathcal{H} \leftarrow \mathcal{H} \cup \{(s^i, w_{\text{norm}}^i, w^i)\}$ 
11    else
12       $\xi \leftarrow$  random sampling from  $[0, 1]$ 
13      if  $\xi > \frac{w^i}{w_{\text{perfect}}}$  then
14         $\mathcal{H} \leftarrow \mathcal{H} \cup \{(s^i, w_{\text{norm}}^i, w^i)\}$ 
15      else
16         $\mathcal{L} \leftarrow \mathcal{L} \cup \{(s^i, w_{\text{norm}}^i, w^i)\}$ 
17      end
18    end
19  /* Normal MCL update for  $\mathcal{H}$  */
20  for  $i = 1$  to  $\|\mathcal{H}\|$  do
21    sample  $h$  from  $\mathcal{H}$  according to  $w_{\text{norm}}^1, \dots, w_{\text{norm}}^{\|\mathcal{H}\|}$ 
22    sample  $h' \sim p(h'|a_{t-1}, h)$ 
23     $w_{h'} = p(o_t|h')$ 
24     $\mathcal{P}_t \leftarrow \mathcal{P}_t \cup (h', w_{h'})$ 
25  end
26  /* Dual MCL update with PM for  $\mathcal{L}$  */
27  for  $i = 1$  to  $\|\mathcal{L}\|$  do
28    sample  $l'$  according to PM
29    sample  $l \sim p(l'|a_{t-1}, l)$ 
30     $w_{l'} = w_l$ 
31     $\mathcal{P}_t \leftarrow \mathcal{P}_t \cup (l', w_{l'})$ 
32  end
33   $w^{\text{norm}} \leftarrow$  normalize  $w \in \mathcal{P}_t$ 
34  return  $\mathcal{P}_t$ 
35 end

```

B Parameter Sensitivity Experiment

We conduct parameter sensitivity experiments on two important parameters in ADAPTIVE MIXTURE MCL: w_{cut} and the number of particles. Results are shown in Figure 7. When we look at (a) in Figure 7, it can be found that the performance of ADAPTIVE MIXTURE MCL is very stable when number of particles varies and ADAPTIVE MIXTURE MCL can converge to the accurate pose even with only 200 particles. This can significantly decrease the computation cost, especially when deployed in large scenes where traditional MCL requires large amount of particles to converge to the accurate pose.

As shown in (b) in Figure 7, when w_{cut} varies, ADAPTIVE MIXTURE MCL achieves good estimation accuracy. When w_{cut} is lower, ADAPTIVE MIXTURE MCL converges slower because it takes more time for the algorithm to recognize the wrong particles. When w_{cut} is higher than 0.8, the estimation accuracy gets “turbulent”. The reason for this phenomenon lies in that with high w_{cut} , the algorithm lacks the ability to endure flaws in the observation and when PM fails to capture the correct pose, many new particles will be sampled at the wrong poses, resulting in higher estimation error and the “turbulent” performance.

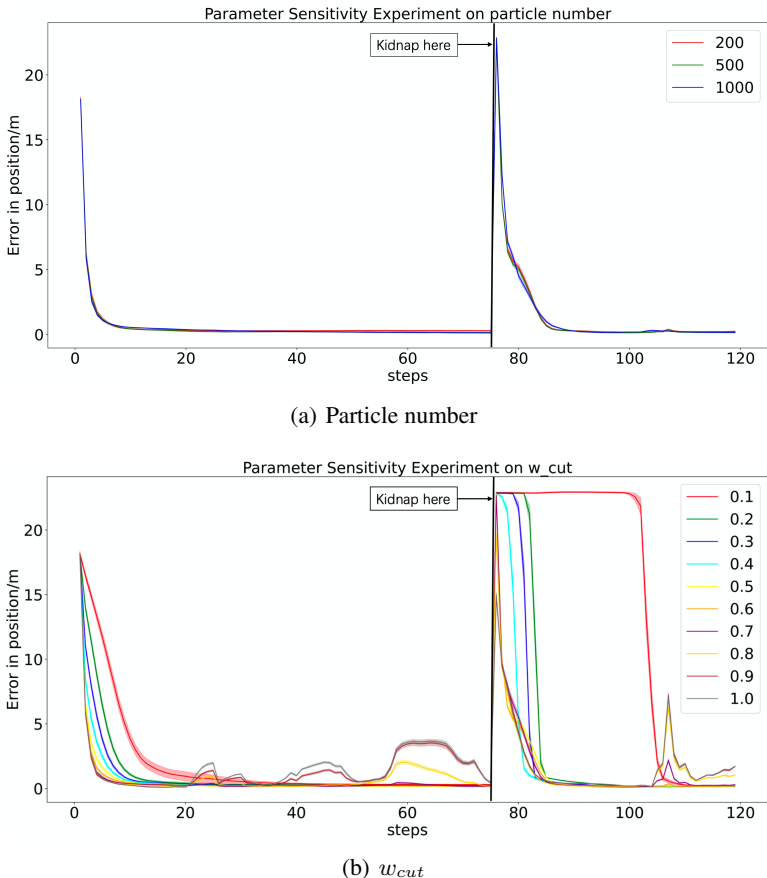


Figure 7: Results on parameter sensitivity experiments

C GT Generation

To generate $\mathbf{GT} \in \mathbb{R}^{H_{env} \times W_{env} \times K}$ for a given pose (x, y, θ) , we begin with an all-zero matrix for \mathbf{GT} . Then a GaussianBlur is deployed on a one-hot ground truth matrix of (x, y) , resulting in $\mathbf{GT}' \in \mathbb{R}^{H_{env} \times W_{env}}$. As θ can usually be different from the angle values in the discretized angle

space, we find the nearest two values (θ_1 and θ_2) to θ and then a linear interpolation is deployed on these two values as described in (12). I_{θ_1} is the index for θ_1 and $\mathbf{GT}_{:::,I_{\theta_1}}$ indicate all the entries where the third indicator equals to I_{θ_1} .

$$\mathbf{GT}_{:::,I_{\theta_1}} = \left| \frac{\theta_1 - \theta}{\theta_1 - \theta_2} \right| \quad (12)$$

$$\mathbf{GT}_{:::,I_{\theta_2}} = 1 - \mathbf{GT}_{:::,I_{\theta_1}}$$

Finally, we aggregate both the position and orientation ground truth as described in (13) and then a normalization is deployed on \mathbf{GT} , leading to the final ground truth.

$$\mathbf{GT}_{i,j,k} = \mathbf{GT}_{i,j,k} \cdot \mathbf{GT}'_{i,j} \quad (13)$$

D More Experiments in synthetic environments.

To demonstrate the robustness of ADAPTIVE MIXTURE MCL, we conduct more experiments in synthetic environments. In the two synthetic environments where we collect testing sequences, we generate 20 random testing sequences, each of which contains one kidnapping. Figure 8 illustrates 6 testing sequences among these 20, where red lines are two trajectories before and after kidnapping.

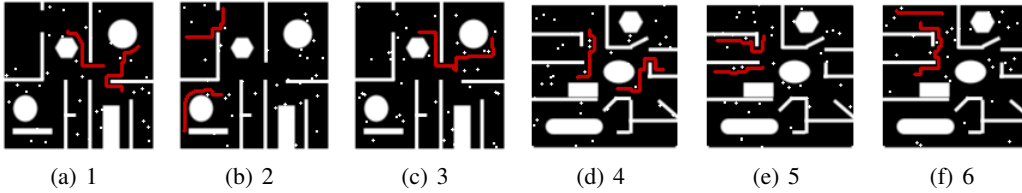


Figure 8: Trajectories in synthetic environments.

600 experiments are conducted on these 20 sequences. Results for position error and converging steps are respectively shown in Figure 9 and 10. It can be found that ADAPTIVE MIXTURE MCL achieves much more accurate position estimation results as compared to MIXTURE MCL and MCL. Also ADAPTIVE MIXTURE MCL converges the fastest and attains the highest converging rate.

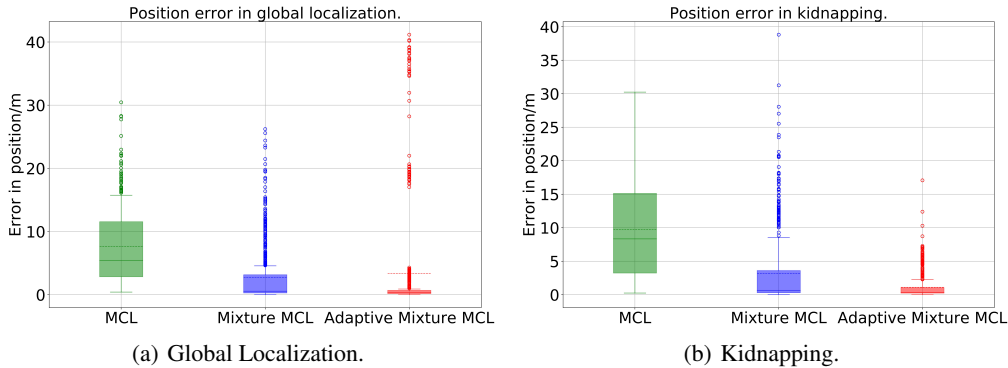


Figure 9: The results for position error in global localization and kidnapping problem among 600 experiments.

E Bays Filtering

Here we make a brief summary for the probability framework introduced in Monte Carlo Localization [7], the heart of which is the Recursive Bayes Filtering. Bayes filter naturally introduces an

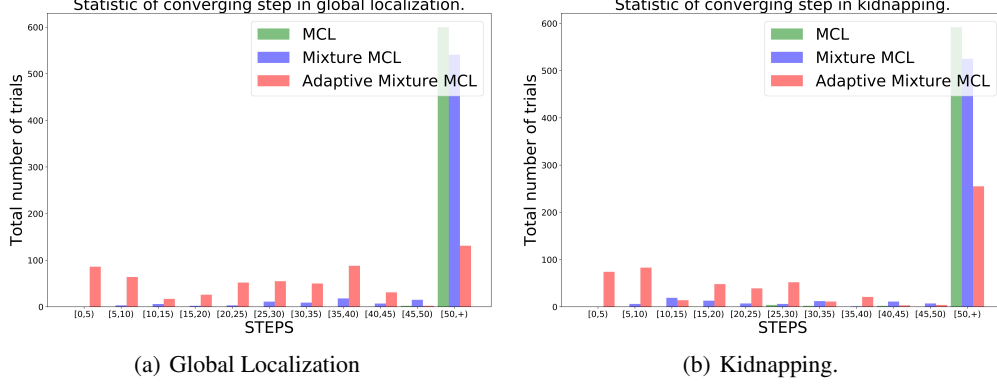


Figure 10: Histograms for converging steps among 600 experiments in global localization and kidnapping problem.

Markov assumption on the environment, that is the observation in the environment only depends on the current state if the state is known. As shown in (14), the possibility distribution $Bel(s_t)$ is a conditional possibility density over the whole sequence of observation information and motion information.

$$Bel(s_t) = p(s_t | o_{0:t}, a_{0:t-1}, \mathbf{M}_{env}) \quad (14)$$

According to the Bayes Theorem [17] [18], we deploy Bayes rule on (14) and transform it into (15), where η is the normalization term in Bayes rule.

$$Bel(s_t) = \frac{p(o_t | s_t, a_{0:t-1}, o_{0:t-1}, \mathbf{M}_{env}) p(x_t | a_{0:t-1}, o_{0:t-1}, \mathbf{M}_{env})}{p(o_t | s_t, a_{0:t-1}, o_{0:t-1}, \mathbf{M}_{env})}$$

$$\eta = \frac{1}{p(o_t | s_t, a_{0:t-1}, o_{0:t-1}, \mathbf{M}_{env})} \quad (15)$$

$$Bel(s_t) = \eta p(o_t | s_t, a_{0:t-1}, o_{0:t-1}, \mathbf{M}_{env}) p(s_t | a_{0:t-1}, o_{0:t-1}, \mathbf{M}_{env})$$

The second term in (15) can be simplified as shown in (16) because Bayes filter assumes that the environment is Markov.

$$p(o_t | s_t, a_{0:t-1}, o_{0:t-1}, \mathbf{M}_{env}) = p(o_t | s_t, \mathbf{M}_{env}) \quad (16)$$

Also, the third term in (15) can be expanded by integrating over the state at time stamp $t-1$, as described in (17).

$$p(s_t | a_{0:t-1}, o_{0:t-1}, \mathbf{M}_{env}) = \int p(s_t | s_{t-1}, a_{0:t-1}, \mathbf{M}_{env}) p(s_{t-1} | a_{0:t-1}, o_{0:t-1}, \mathbf{M}_{env}) ds_{t-1} \quad (17)$$

Thus, we have the following equation for what we have so far about the probability distribution of the pose of the robot.

$$Bel(s_t) = \eta p(o_t | s_t, \mathbf{M}_{env}) \int p(s_t | s_{t-1}, a_{0:t-1}, \mathbf{M}_{env}) p(s_{t-1} | a_{0:t-1}, o_{0:t-1}, \mathbf{M}_{env}) ds_{t-1} \quad (18)$$

Applying the Markov assumption again, we can make the first term inside the integration simple in (19).

$$p(s_t | s_{t-1}, a_{0:t-1}, \mathbf{M}_{env}) = p(s_t | s_{t-1}, a_{t-1}, \mathbf{M}_{env}) \quad (19)$$

(20) summaries the recursive Bayes filter for computing the possibility distribution $Bel(s_t)$ of the robot pose, where η is the normalization term, $p(o_t | s_t)$ stands for the Observation Model, $p(s_t | s_{t-1}, a_{t-1})$ describes the Motion Model and $Bel(s_{t-1})$ stands for the Prior (distribution at

the last time stamp).

$$\begin{aligned} Bel(s_t) &= \eta p(o_t | s_t, \mathbf{M}_{env}) \int p(s_t | s_{t-1}, a_{t-1}, \mathbf{M}_{env}) p(s_{t-1} | a_{0:t-1}, o_{0:t-1}, \mathbf{M}_{env}) ds_{t-1} \\ &= \eta p(o_t | s_t, \mathbf{M}_{env}) \int p(s_t | s_{t-1}, a_{t-1}, \mathbf{M}_{env}) Bel(s_{t-1}) ds_{t-1} \end{aligned} \tag{20}$$